Biological Psychiatry: GOS

Archival Report

Perineuronal Nets in the Dorsomedial Striatum Contribute to Behavioral Dysfunction in Mouse Models of Excessive Repetitive Behavior

Brandy A. Briones, Miah N. Pitcher, Weston T. Fleming, Alexandra Libby, Emma J. Diethorn, Amanda E. Haye, Camden J. MacDowell, Anna D. Zych, Renée C. Waters, Timothy J. Buschman, Ilana B. Witten, and Elizabeth Gould

ABSTRACT

BACKGROUND: Excessive repetitive behavior is a debilitating symptom of several neuropsychiatric disorders. Parvalbumin-positive inhibitory interneurons in the dorsal striatum have been linked to repetitive behavior, and a sizable portion of these cells are surrounded by perineuronal nets (PNNs), specialized extracellular matrix structures. Although PNNs have been associated with plasticity and neuropsychiatric disease, no previous studies have investigated their involvement in excessive repetitive behavior.

METHODS: We used histochemistry and confocal imaging to investigate PNNs surrounding parvalbumin-positive cells in the dorsal striatum of 4 mouse models of excessive repetitive behavior (BTBR, Cntnap2, Shank3, prenatal valproate treatment). We then investigated one of these models, the BTBR mouse, in detail, with DiI labeling, in vivo and in vitro recordings, and behavioral analyses. We next degraded PNNs in the dorsomedial striatum (DMS) using the enzyme chondroitinase ABC and assessed dendritic spine density, electrophysiology, and repetitive behavior.

RESULTS: We found a greater percentage of parvalbumin-positive interneurons with PNNs in the DMS of all 4 mouse models of excessive repetitive behavior compared with control mice. In BTBR mice, we found fewer dendritic spines on medium spiny neurons (targets of parvalbumin-positive interneurons) and differences in neuronal oscillations as well as inhibitory postsynaptic potentials compared with control mice. Reduction of DMS PNNs in BTBR mice altered dendritic spine density and inhibitory responses and normalized repetitive behavior.

CONCLUSIONS: These findings suggest that cellular abnormalities in the DMS are associated with maladaptive repetitive behaviors and that manipulating PNNs can restore normal levels of repetitive behavior while altering DMS dendritic spines and inhibitory signaling.

https://doi.org/10.1016/j.bpsgos.2021.11.005

Maladaptive repetitive behavior is a common symptom of several neuropsychiatric disorders, including autism spectrum disorder, schizophrenia, obsessive-compulsive disorder, and other anxiety-related psychopathologies (1–5). These symptoms impair everyday living throughout the lifespan and likely increase the severity of other symptoms, such as impaired cognition and social deficits (1–5). In humans, studies have linked repetitive and inflexible behaviors with corticostriatal circuits (6–9), where impairments in modulatory function are hypothesized to exacerbate symptom severity. Rodent dorsal striatum dysfunction has been linked to aberrant repetitive behaviors (10–12), including self-injurious overgrooming and excessive digging.

The dorsal striatum seems homogeneous in its cellular structure, where a striking 95% of its neurons are GABAergic (gamma-aminobutyric acidergic) medium spiny neurons (MSNs), while the other 5% of striatal neurons consist of various interneuron subtypes (e.g., GABAergic, cholinergic) (13–15). One of the larger subpopulations of GABAergic interneurons in the striatum are parvalbumin-positive (PV+) fast-spiking interneurons (16–18). These interneurons modulate extrastriatal excitatory input to MSNs, where inhibition from small populations of PV+ interneurons can downregulate the activity of large populations of MSNs (19,20).

Most dorsal striatal PV+ interneurons are surrounded by perineuronal nets (PNNs) (21), specialized extracellular matrix structures important for plasticity (22–25) and development (26,27). Recent studies have implicated PNNs and PV+ cells in neuropsychiatric diseases, including schizophrenia, autism spectrum disorder, and Alzheimer's disease (28–31), and mutations in extracellular matrix–related genes have been identified in genome-wide association studies of humans with autism spectrum disorder (32,33). These results suggest that PNNs play an important role in regulating PV+ interneurons and thereby plasticity and neuropsychiatric symptoms. However, no studies have investigated whether PNNs in the dorsal

ISSN: 2667-1743

striatum play a role in excessive repetitive behavior in mouse models.

We examined the distribution of PNNs in the dorsomedial striatum (DMS) and dorsolateral striatum (DLS) of 4 mouse models known to exhibit excessive repetitive behavior—BTBR, Cntnap2$^{-/-}$, Shank3$^{+/-\Delta C}$, and prenatal exposure to valproic acid (VPA)—and found consistent increases in the percentage of PV+ interneurons surrounded by PNNs in the DMS compared with control mice, raising the possibility that this increase restricts plasticity. To test this hypothesis, we investigated multiple plasticity measures in the DMS of BTBR and healthy control mice. DMS MSNs showed reduced dendritic spines and enhanced inhibitory presynaptic strength ex vivo in BTBR mice compared with healthy control mice, as well as altered in vivo neuronal oscillations linked to PV+ interneurons recorded during grooming and digging behavior. These results suggest that PNNs surrounding PV+ interneurons may disrupt inhibitory signaling in BTBR mice. To test this, we degraded DMS PNNs in BTBR mice and found that this manipulation was sufficient to restore control levels of MSN dendritic spines, alter inhibitory transmission, and partially rescue excessive grooming and digging behavior. Together, these findings suggest that the increased percentage of PV+ interneurons with PNNs may interfere with optimal synaptic plasticity in the DMS, contributing to maladaptive repetitive behaviors.

METHODS AND MATERIALS

Animals

All animal procedures were conducted in accordance with the National Institutes of Health guidelines and approved by the Princeton University Institutional Animal Care and Use Committee. C57BL/6J mice (strain 000664) and inbred strain BTBR T+Itpr3tf/J mice (strain 002282) were obtained from The Jackson Laboratory and used for behavior, histological, and physiological comparisons. Transgenic mice, Cntnap2$^{-/-}$ (strain 017482) and Shank3$^{+/-\Delta C}$ (strain 018398), were used for histology. VPA-treated mice were genotype C57BL/6J-Tg(Thy1-GCaMP6f)GP5.3Dkim/J (strain 028280) and used for histology.

Stereotaxic Surgery

C57BL/6 and BTBR mice were anesthetized with 1% to 2% isoflurane and placed in a stereotaxic setup (David Kopf Instruments). A microsyringe and pump (World Precision Instruments) were used to deliver enzyme, chondroitinase ABC (chABC) or penicillinase (pnase), to the bilateral DMS. For in vivo local field potential (LFP) recordings, a tetrode was implanted in the DMS unilaterally (see Supplemental Methods). Behavior was quantified 10 days after surgery.

Behavioral Testing

C57BL/6 and BTBR mice were scored for spontaneous grooming and digging as measures of repetitive behavior. Mice were placed in a dark open field apparatus inside an empty operant chamber (Med Associates Inc.) with an overhead video camera. The day before testing, mice were habituated to the open field apparatus twice for 5 minutes each. Grooming and digging tests were 10 minutes each, and order was counterbalanced.

In Vivo Local Field Potential Recording

Mice were habituated to wearing the 140× gain wireless head stage (Triangle Biosystems) in their home cage twice for 5 minute each. Mice were placed in a red-lit open field apparatus with bedding for 10 minutes with an overhead video camera to time lock grooming and digging behavior with recording data. Neural data were transmitted to a wireless receiver and recorded using NeuroWare software (Triangle Biosystems). All recordings referenced a silver wire wrapped around the ground screw implanted in the posterior parietal bone. LFPs were extracted from each animal's electrophysiological data using MATLAB 2016b (The MathWorks, Inc.). Python 3.7 (Python Software Foundation) was used for all subsequent analyses and plots of LFP data (see Supplemental Methods).

Slice Electrophysiology

Whole-cell recordings were performed with a Multiclamp 700B (Molecular Devices) from 300-μm coronal slices through the DMS. Whole-cell currents were filtered at 1 kHz and digitized and stored at 20 kHz (Clampex 9; MDS Analytical Technologies). All experiments were completed within 4 hours after slices were made to maximize cell viability and consistency.

Miniature inhibitory postsynaptic currents (mIPSCs) were recorded in the presence of tetrodotoxin (1 μM), d-AP5 (50 μM), and NBQX (20 μM) in the recording artificial cerebrospinal fluid solution. mIPSC data were analyzed with Stimfit (34) using a detection threshold of >7 pA. For each cell, a stretch of 250 mIPSCs was analyzed, with data collection beginning 5 to 10 minutes after patching onto each cell. For confirmation that currents were exclusively inhibitory, picrotoxin (100 μM) was added to the bath after recordings.

Histology

Mice were transcardially perfused with 4.0% paraformaldehyde, and brains were dissected and postfixed. Histochemistry was carried out on 50-μm-thick free-floating coronal brain sections incubated in primary antibodies against PV, choline acetyltransferase, calretinin, neuropeptide Y, glial fibrillary acid protein, and/or biotinylated lectin *Wisteria floribunda* agglutinin (WFA) and counterstained with DAPI (Table S5). For the chABC-behavior experiment, sections were imaged with a NanoZoomer S60 (Hamamatsu), and all other sections were imaged with a Zeiss LSM 700 confocal microscope (Carl Zeiss AG).

DiI Labeling

MSN dendritic spine labeling was carried out on 80-μm-thick coronal brain sections. As previously described (35), individual sections were labeled with lipophilic membrane DiI-coated tungsten particles using a Helios Gene Gun system (Bio-Rad Laboratories) and incubated at 4 °C for 24 hours in 0.1M phosphate-buffered saline. Sections were then postfixed in

4% paraformaldehyde for 1 hour at room temperature before imaging.

Confocal Microscopy

Images were acquired using a Zeiss LSM 700 confocal microscope. Brain sections for comparison were stained together; all images were taken with near-identical confocal settings and were equally sampled to allow for cross-comparisons. For PV+WFA+, PV+, and WFA+ cell density analyses, 4 to 6 sections (1:6 series) of the DMS were imaged (20× with 0.5× zoom; numerical aperture, 0.8) taking z-stacks at 3.0-μm intervals (approximately 16 optical slices per cell). For DiI analyses, dendritic secondary and tertiary segments were imaged (63× with oil at 2.0× zoom; numerical aperture, 1.4) taking z-stacks at 0.2-μm intervals. Slides were coded before analysis, and the code was not revealed until the analysis was complete. All images were analyzed using Fiji (36); https://imagej.nih.gov/ij/.

Statistical Analysis

Statistics used throughout the article include linear mixed-effects modeling, analyses of variance, *t* tests, and shuffle tests, as described in figure legends (see Supplemental Methods and data tables in Supplement).

RESULTS

Mouse Models of Excessive Repetitive Behavior Have Higher Percentage of PV+ Interneurons With PNNs in the DMS

Using fluorescent tagged WFA to label PNNs combined with immunolabeling for PV, we observed PV+WFA+ interneurons throughout the dorsal striatum in 4 mouse models: BTBR, Cntnap2$^{-/-}$, Shank3$^{+/-\Delta C}$, and VPA-treated (Figure 1D), each known to exhibit excessive repetitive behaviors (37–42). A greater percentage of PV+ interneurons colocalized with WFA was observed in the DMS for all mouse models compared with respective age-matched control mice (BTBR: $p = .0204$, Cntnap2$^{-/-}$: $p = .0195$, Shank3$^{+/-\Delta C}$: $p = .0041$, VPA: $p = .0445$) (Figure 1A–C; Table S1). By contrast, we found no WFA-PV colocalization differences in the DLS (Figure 1A–C). Similarly, we found no evidence of increased overall WFA+ cell density in either the DMS or the DLS (Figure 1E–G; Table S1), with the exception that BTBR mice had a greater number of WFA+ cells in the DLS compared with control mice ($p = .0186$) (Figure 1E). No WFA+ labeling was found surrounding choline acetyltransferase–positive, calretinin-positive, or neuropeptide Y–positive interneuron types in the dorsal striatum (Figure S1A, B), similar to a previous study (21).

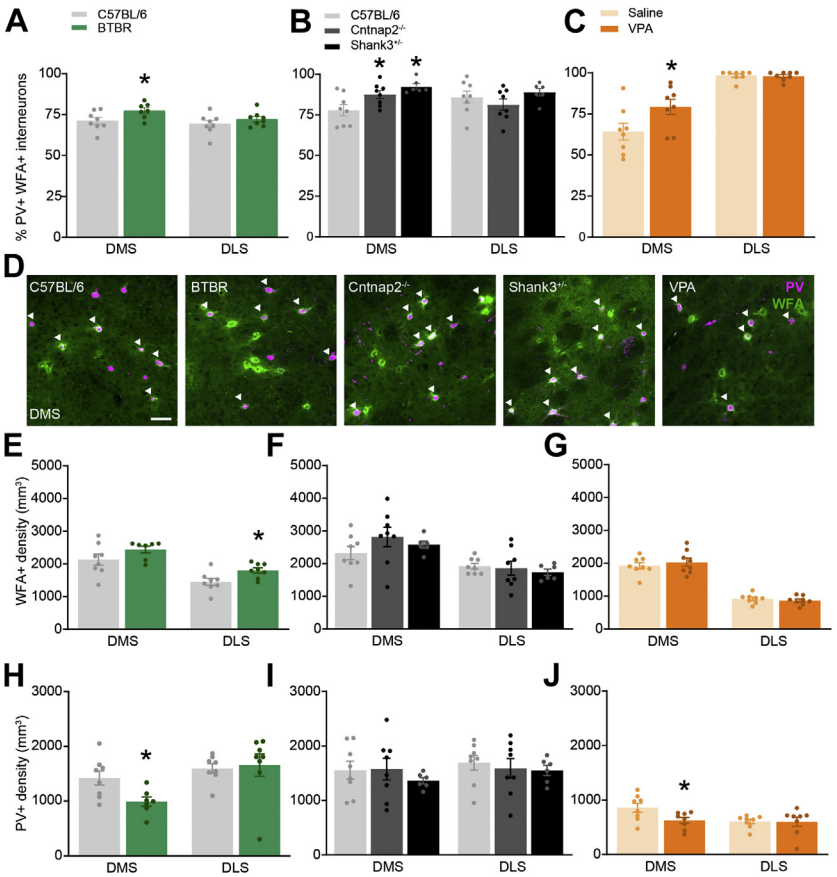

Figure 1. Mouse models with excessive repetitive behaviors have more DMS PV+ interneurons with PNNs. **(A–C)** Histological analysis of WFA+ PNNs and PV+ interneurons revealed an increase in DMS percent colocalization compared with control mice in BTBR mice ($p = .0204$) **(A)**, Cntnap2$^{-/-}$ mice ($p = .0195$) and Shank3$^{+/-\Delta C}$ mice ($p = .0041$) **(B)**, and VPA-treated mice ($p = .0445$) **(C)**. No differences were found in the DLS **(A–C)**. **(D)** Representative images of PV+ interneurons (magenta) and WFA+ PNNs (green) in the DMS. White triangles indicate PV+WFA+ cells. Scale bar = 50 μm. **(E–G)** No differences were found in WFA+ PNN density in DMS of BTBR mice **(E)**, Cntnap2$^{-/-}$ and Shank3$^{+/-\Delta C}$ mice **(F)**, or VPA mice **(G)**. DLS PNN+ density was higher in BTBR mice compared with control mice ($p = .0186$) **(E)**, but not in Cntnap2$^{-/-}$ and Shank3$^{+/-\Delta C}$ mice **(F)** or VPA mice **(G)**. PV+ density was lower in the DMS of BTBR ($p = .0187$) and VPA ($p = .0379$) mice compared with respective control mice, but not in Cntnap2$^{-/-}$ or Shank3$^{+/-\Delta C}$ mice. **(H–J)** No differences were detected in the DLS of BTBR mice **(H)**, Cntnap2$^{-/-}$ and Shank3$^{+/-\Delta C}$ mice **(I)**, or VPA-treated mice **(J)**. Data are represented as mean ± SEM. See also Figure S1. See Table S1 for complete statistics. *$p < .05$. DLS, dorsolateral striatum; DMS, dorsomedial striatum; PNN, perineuronal net; PV, parvalbumin; VPA, valproic acid; WFA, *Wisteria floribunda* agglutinin.

BTBR and VPA-treated mice had fewer PV+ expressing interneurons in the DMS (BTBR: $p = .0187$, VPA: $p = .0379$) (Figure 1H–J; Table S1). Tyramide amplification of PV+ protein expression in BTBR mice replicated this difference ($p = .0331$, BTBR: 454.47 ± 76.97 cells/mm^3, control: 996.38 ± 107.9 cells/mm^3), suggesting that BTBR and VPA-treated mice have reduced PV+ interneuron densities, not just decreased PV+ protein expression. Overall, when controlling for density differences, PV+ interneurons were more likely to be surrounded by WFA+ labeling in all 4 mouse models compared with control mice (Figure 1A–C; Table S1).

Excessive Grooming and Digging Behavior Are Diminished in BTBR Mice by Reducing DMS PNNs

We decided to focus the remainder of our studies on the BTBR model, an inbred strain, given their robust and replicable behavior phenotypes and that most psychopathologies with excessive repetitive behavior manifest as idiopathic. We characterized grooming and digging behavior in BTBR mice compared with control mice (Figure 2A), and as expected (43–45), we found that BTBR mice spent more time grooming ($p = .0222$) and engaged in longer grooming bouts ($p < .0001$) (Figure S2A; Table S5). BTBR mice also spent more time digging ($p = .0413$) and initiated a greater number of digging bouts ($p = .0123$) (Figure S2B; Table S5).

To test whether PNNs play a role in high levels of repetitive behaviors, we used chABC to degrade PNNs in the DMS. Previous studies have used chABC in various brain regions in adult mice (29,46–48), where it has transient effects on PNNs. To characterize the effect of chABC on PNNs in the DMS, we unilaterally infused chABC in one hemisphere and a control enzyme, pnase, in the other (Figure S3A). We found an almost

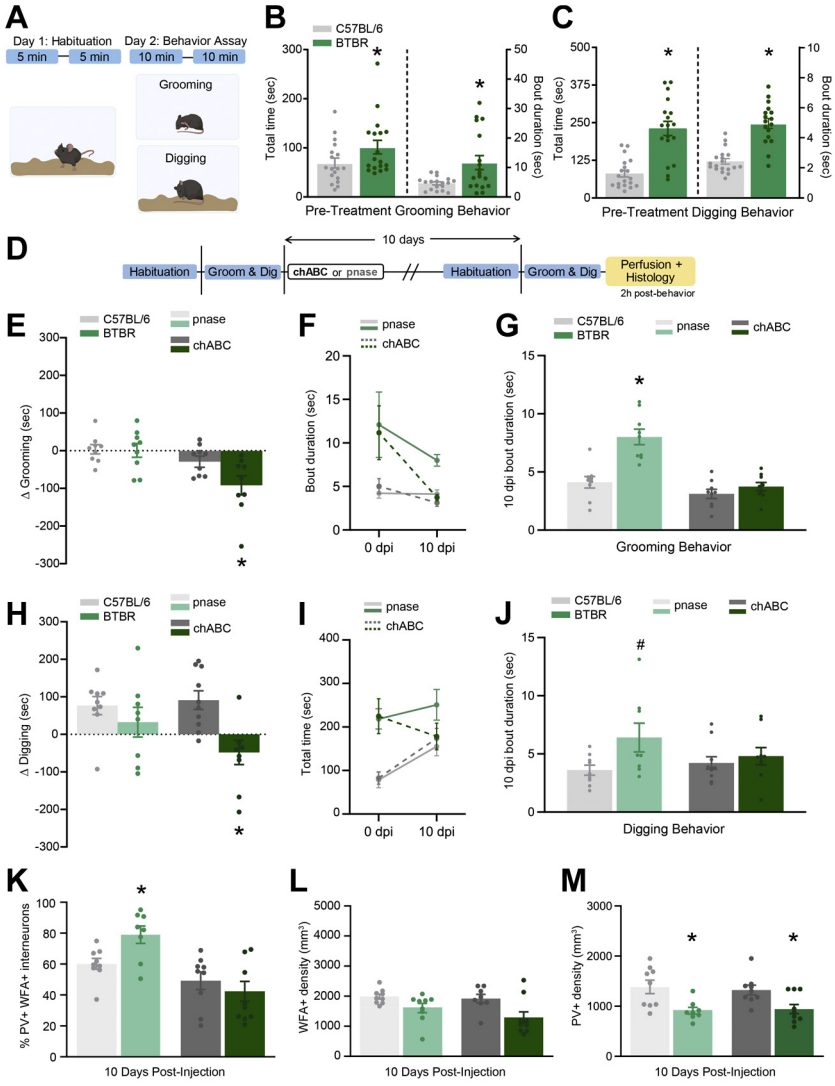

Figure 2. Reducing PNNs in DMS rescues excessive repetitive behaviors and normalizes grooming and digging behaviors in BTBR mice. **(A)** Mice were habituated to an enclosed open field box twice for 5 minutes a day before behavioral testing. The next day mice were tested in both open field grooming and thick bedding digging paradigm (order counterbalanced). **(B)** BTBR mice showed elevated time spent grooming compared with control mice ($p = .0293$) and longer time spent grooming per bout ($p = .0202$). **(C)** BTBR mice showed greater time spent digging compared with control mice ($p < .0001$) and longer time spent digging per bout ($p < .0001$). **(D)** Experiment timeline of behavior pre-injection, stereotaxic surgery, behavior post-injection, and tissue collection for histology. **(E)** Mean change (Δ) in time spent grooming from pre- to postinjection per mouse. Negative values depict a decrease in time spent, and positive values depict an increase in time spent, where means near zero (dashed line) represent no change in behavior from pre- to postinjection. BTBR-chABC mice show decreases in grooming (Δ−91.44 ± 25.43 seconds), a significant change compared with the control group ($p = .0036$). **(F, I)** Graphical representation of the mean bout duration from pre- to postinjection. **(G)** 10 dpi of chABC in the DMS normalized BTBR grooming bout duration (3.73 ± 0.36 seconds), comparable to C57BL/6 mice (3.11 ± 0.39 seconds), while 10 dpi of pnase in BTBR mice maintained prolonged grooming bouts (8.00 ± 0.66 seconds) ($p = .0014$). **(H)** Mean Δ in time spent digging from pre- to postinjection shows a decrease in BTBR-chABC mice (Δ−62.36 ± 32.88 seconds), a significant change compared with control mice ($p = .0295$). **(J)** 10 dpi of chABC in the DMS of BTBR mice normalized digging bout duration (4.81 ± 0.74 seconds), comparable to C57BL/6 mice (4.22 ± 0.54 seconds). **(K)** Histological analysis of DMS WFA+ labeled PNNs confirms reduction in the percent of PV+ interneurons positive for PNNs in BTBR-chABC mice. BTBR-pnase mice show an increase in percent of PV+ interneurons positive for PNNs compared with C57BL/6-pnase mice ($p = .023$), **(L)** with no differences in overall WFA+ cell density. **(M)** PV+ density was lower in BTBR mice compared with control mice in both chABC ($p = .0009$) and pnase ($p = .0028$) treatment groups. Data are represented as mean ± SEM. See also Figure S2 and S3. See Table S2 for complete statistics. *$p < .05$; #$p < .075$. chABC, chondroitinase ABC; DMS, dorsomedial striatum; dpi, days post injection; pnase, penicillinase; PNN, perineuronal net; PV, parvalbumin; WFA, *Wisteria floribunda* agglutinin.

complete degradation of PNNs in the DMS at 4 days post injection (dpi), approximately 60% regrowth at 7 dpi, and complete recovery by 21 dpi (Figure S3B, D), with no effect on PV+ interneuron expression (Figure S3C). Based on these results, we selected a 10 dpi time point as a time when BTBR PV+ PNN+ colocalization would be most similar to control-like levels.

Before chABC injection, we obtained baseline levels of grooming and digging in BTBR and control mice. BTBR mice spent more time grooming ($p = .0293$) and had longer grooming bouts ($p = .0202$) (Figure 2B; Table S2). BTBR mice also spent more time digging ($p < .0001$) and had longer digging bouts ($p < .0001$) (Figure 2C; Table S2). These mice were then randomly assigned to groups receiving bilateral DMS injections of either chABC or control enzyme pnase.

At 10 dpi, grooming and digging behaviors were quantified again (Figure 2D). Diminishing PNNs in the DMS of BTBR mice significantly reduced their time spent grooming compared with grooming behavior before chABC injection ($p = .007$) (Figure 2E; Table S2). Grooming behavior was not statistically different in control mice treated with either chABC or pnase and in BTBR mice treated with pnase (Figure 2E). Diminishing PNNs in the DMS of BTBR mice also reduced their time spent grooming within a bout so that this behavior was not statistically different from control groups (Figure 2F, G; Table S2). BTBR mice with DMS injection of pnase maintained high amounts of grooming bout time before and after injection, while control mice treated with chABC showed no significant differences (Figure 2E–G; Table S2). Similarly, chABC treatment of BTBR mice reduced their time spent digging from pre- to postinjection compared with control groups (Figure 2H, I; Table S2) and reduced their time spent digging within a bout so that their behavior was not statistically different from control mice (Figure 2J; Table S2). Altogether, DMS injection of chABC reduced BTBR grooming and digging behavior to levels comparable to control mice.

To assess chABC and pnase effects on PV+ interneurons and WFA+ PNNs in the DMS, we analyzed PNN levels using WFA. At 10 dpi, pnase-injected BTBR mice showed a higher percentage of PV+ interneurons with WFA labeling compared with pnase-injected control mice ($p = .0235$), whereas chABC-injected BTBR mice showed no difference compared with chABC-injected control mice ($p = .359$) (Figure 2K; Table S2). No differences were seen when analyzing WFA+ cell density (Figure 2L; Table S2). Similar to our previous results, BTBR mice showed significantly lower PV+ cell density compared with control mice in both chABC-treated ($p = .0093$) and pnase-treated ($p = .0028$) groups (Figure 2M; Table S2).

BTBR Mice Show Atypical Neuronal Oscillations, Inhibitory Signaling, and Dendritic Spines in the DMS

Patterns of oscillatory activity in the striatum have been hypothesized to arise from rhythmic firing of PV+ cells and have been linked to voluntary striatum-dependent behaviors (49,50). During freely moving behavior sessions, we recorded LFPs from the DMS of BTBR and control mice (Figure 3A). LFP recordings were time-locked to analyze LFPs just before the initiation of, during the course of, or just before termination of a grooming or digging bout. For both grooming and digging, we found differences in LFP power (mV^2/Hz) during the pre-event period. Before the initiation of grooming, BTBR mice showed higher LFP power within the theta frequency band (4–12 Hz) ($p \leq .001$) compared with control mice (Figure 3B; Table S3), while prior to the initiation of digging, LFP power in the low (30–80 Hz) and high (>80 Hz) gamma frequencies was higher in BTBR mice ($p \leq .01$) (Figure 3E; Table S3). During grooming, BTBR mice again showed higher theta power ($p \leq .001$) as well as lower gamma power (30–80 Hz) ($p \leq .01$) compared with control mice (Figure 3C; Table S3). Toward the end of the grooming event, this pattern persisted, with BTBR mice showing higher theta power ($p \leq .01$) and lower gamma power ($p \leq .001$) compared with control mice (Figure 3D; Table S3). These differences were not observed throughout the digging events, perhaps reflecting differences in the degree to which grooming and digging are purposeful behaviors (Figure 3F, G; Table S3). Our LFP observations in combination with our PNN and chABC data suggest a potential role for PV+ PNN+ interneurons in modulating excessive grooming by altering oscillatory behavior.

PV+ cells provide an important source of inhibition onto MSNs in the dorsal striatum, so we used slice electrophysiology to investigate inhibitory transmission onto DMS MSNs of BTBR and control mice (Figure 3H). We recorded mIPSCs at presumed MSNs in unoperated untested mice to determine whether differences exist in inhibitory synaptic input and strength. Comparison of overall mIPSC mean frequencies (Hz), a measure indicative of inhibitory presynaptic strength, yielded no differences between groups (Figure 3I; Table S3). However, comparison of mIPSC mean amplitudes (pA), a measure indicative of inhibitory postsynaptic strength, revealed a significant difference between BTBR and control mice. BTBR mice showed an increase in mean amplitude of mIPSC events relative to control mice (Figure 3J; Table S3). This effect may be mediated by increases in frequency of high-amplitude (>60 pA) events (Figure 3K). These higher amplitudes are thought to be representative of events proximal to the soma, a location where PV+ interneurons synapse onto MSNs (19,51). Our mIPSC observations in the BTBR model suggest the presence of particularly strong inhibitory responses at MSNs not seen in control mice.

In addition to receiving inhibitory input, the DMS has been shown to integrate a heterogeneous set of inputs from prefrontal cortex, premotor cortex, and thalamus (52), where MSNs receive specific excitatory inputs from these extrastriatal regions onto dendritic spines (53,54). Using lipophilic DiI labeling, we examined MSN dendritic spine density in BTBR and control mice (Figure 3L) and found fewer spines on secondary and tertiary dendrites of MSNs in the DMS ($p = .0048$), but not the DLS, of BTBR mice (Figure 3M; Table S3).

Reducing DMS PNNs of BTBR Mice Increases Inhibition and Eliminates Dendritic Spine Differences

To understand how reducing PNNs may affect inhibitory synaptic strength in BTBR and control mice, we recorded mIPSCs from MSNs after chABC injection (Figure 4B). Given differences in percentage of PV+ cells with PNNs between BTBR

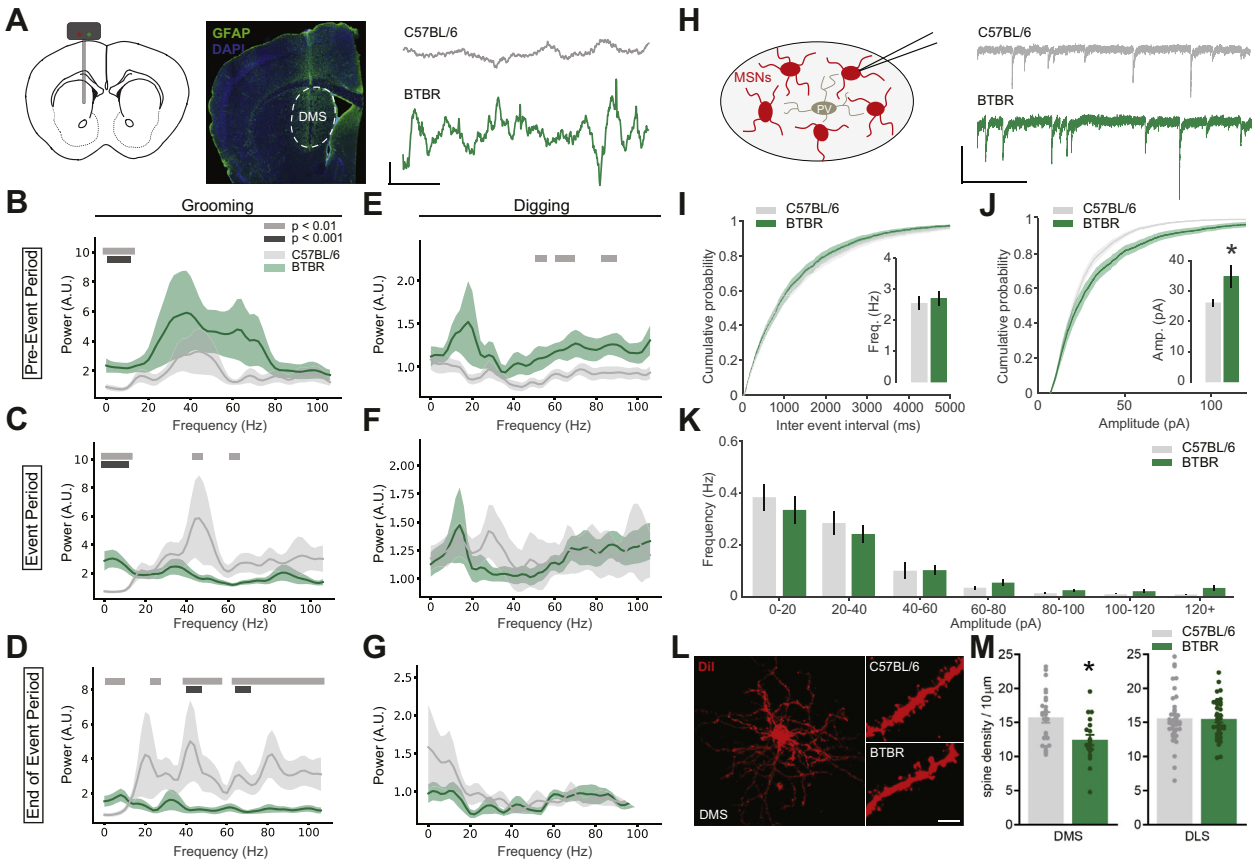

Figure 3. BTBR mice exhibit altered neuronal oscillations, inhibitory transmission, and dendritic spine density in the DMS. **(A)** All mice were implanted unilaterally with an electrode array targeting the DMS. Targeting was confirmed histologically with GFAP and DAPI labeling. Example local field potential traces of a C57BL/6 (top, gray) and a BTBR (bottom, green) mouse. Scale bar = 200 mV (y-axis) by 0.2 second (x-axis). **(B–D)** Normalized local field potential power spectrum data for grooming behavior during the pre-event period (−1 to 0 second prior to event start) **(B)**, event period (0 to 1 second) **(C)**, and end of event period (0 to 1 second prior to event end) **(D)**. **(E–G)** Normalized local field potential power spectrum data for digging behavior during the pre-event period **(E)**, event period **(F)**, and end of event period **(G)**. Gray bars indicate significant differences in power (A.U.) across frequency (Hz): light gray ($p \leq .01$); dark gray ($p \leq .001$). **(H)** Example depiction and traces of whole-cell, mIPSC recordings from putative MSNs of a C57BL/6 (top, gray) and a BTBR (bottom, green) mouse. Scale bar = 40 pA (y-axis) by 2 seconds (x-axis). **(I)** mIPSC frequency (Hz) analysis of C57BL/6 (gray) and BTBR (green) mice data from DMS slice preparations yields no differences in mean frequencies. **(J)** Significant effect in amplitude (pA) of mIPSC events shows increased mean amplitudes in BTBR mice compared with C57BL/6 mice ($p = .0335$). **(K)** Bar graph of mean frequency by amplitude depicts the increased frequency of events at amplitudes >60 pA in BTBR mice. **(L)** Representative images of MSN cell (left panel) and dendritic segments (DiI, red) in the DMS from a control (top right panel) and BTBR (bottom right panel) mouse. Scale bar = 5 µm. **(M)** Spine density differences between C57BL/6 and BTBR mice were observed in the DMS ($p = .0048$), but not in the DLS. Data are represented as mean ± SEM. See Table S3 for complete statistics. *$p < .05$. Amp., amplitude; A.U., arbitrary units; DLS, dorsolateral striatum; DMS, dorsomedial striatum; Freq, frequency; GFAP, glial fibrillary acid protein; mIPSC, miniature inhibitory postsynaptic current; MSN, medium spiny neuron.

and control mice, we hypothesized that chABC may affect BTBR mice differently from controls. Mice were injected bilaterally with chABC into the DMS; then 10 dpi, brain slices were collected for mIPSC measurements at presumed MSNs (Figure 4A). When comparing mIPSC mean frequencies across BTBR mice and control mice 10 days following chABC, we found a significant overall increase in event frequency in BTBR mice ($p = .00126$) (Figure 4C; Table S4), indicative of a strengthening of presynaptic inhibition. Elevated mIPSC amplitudes in BTBR mice compared with control mice persisted following chABC treatment ($p = .0146$) (Figure 4D; Table S4). Cumulative probability curves and frequency distributions of the mIPSC amplitude data show increased frequency in BTBR mice relative to control mice across all amplitude bins (Figure 4D, E), suggesting an increase in inhibitory presynaptic strength that may not be specific to distal or proximal inputs. Overall, these findings suggest that chABC increases inhibitory transmission in BTBR mice compared with control mice, possibly through a widespread, nonspecific enhancement of presynaptic strength.

To investigate whether reducing PNNs affects excitatory input onto MSNs, we examined MSN dendritic spine density in BTBR and control mice at 10 dpi of chABC and pnase. We found no differences between BTBR and control mice or between chABC and pnase, although the surgery itself seems to have elevated dendritic spine density (Figure 4F, G; Table S4).

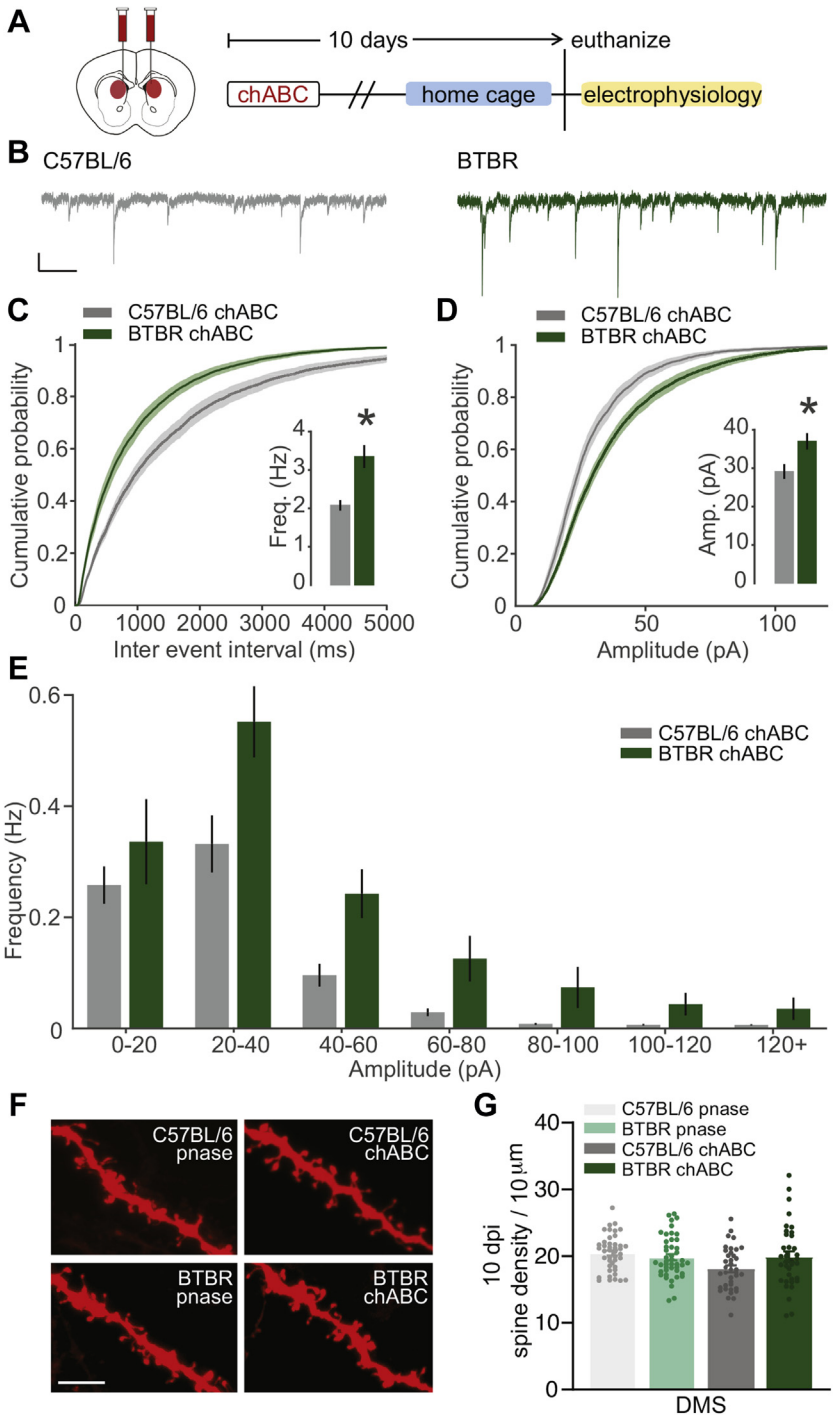

Figure 4. Reducing perineuronal nets alters inhibitory synaptic strength at DMS MSNs and normalizes dendritic spine density. **(A)** Mice were injected bilaterally with chABC in the DMS and lived in their home cage for 10 dpi, and subsequently tissue was collected for slice electrophysiology. **(B)** Example traces of whole-cell, mIPSC recordings from putative MSNs of a C57BL/6 (left, dark gray) and a BTBR (right, dark green) mouse, 10 dpi of chABC. Scale bar = 40 pA (y-axis) by 2 seconds (x-axis). **(C)** mIPSC frequency (Hz) analysis of C57BL/6 and BTBR mice10 dpi of chABC data from DMS slice preparations shows different effects of chABC on C57BL/6 and BTBR mice ($p = .00126$). **(D)** Significant effect in amplitude (pA) of mIPSC events shows increased mean amplitudes in BTBR mice compared with C57BL/6 mice ($p = .0146$). **(E)** Bar graph of mean frequency by amplitude depicts the overall increased frequency of events across amplitudes >20 pA in BTBR mice. **(F)** Representative images of MSN dendritic segments (DiI, red) in the DMS from C57BL/6 mice (top panels), 10 dpi of pnase (top left panel) and 10 dpi of chABC (top right panel) and BTBR mice (bottom panels), 10 dpi of pnase (bottom left panel) and 10 dpi of chABC (bottom right panel). Scale bar = 5 µm. **(G)** Comparison of DMS MSN spine density yields no differences across all groups. Data are represented as mean ± SEM. See Table S4 for complete statistics. *$p < .05$. Amp. amplitude; chABC, chondroitinase ABC; DMS, dorsomedial striatum; dpi, days post injection; Freq, frequency; mIPSC, miniature inhibitory postsynaptic current; MSN, medium spiny neuron; pnase, penicillinase.

DISCUSSION

Our findings show 4 mouse models that exhibit excessive repetitive behavior, namely, BTBR, Cntnap2$^{-/-}$, Shank3, and VPA-treated, have a higher percentage of PV+ interneurons with PNNs in the DMS than control mice. Our data also show altered theta and gamma oscillations (rhythmic firing linked to PV+ cells) during grooming in the DMS of BTBR mice compared with control mice. We also found evidence for increased inhibitory postsynaptic strength on presumed MSNs, the primary target of PV+ cells in the striatum, as well as reduced MSN dendritic spine density in BTBR DMS compared with control

DMS. Diminishing DMS PNNs in BTBR mice reduced both grooming and digging behavior, supporting our hypothesis that PNNs contribute to excessive repetitive behavior. BTBR mice with reduced DMS PNNs showed an unexpected increase in presynaptic inhibition, suggesting that the reduction in repetitive behavior with diminished DMS PNNs is not the result of a normalization of inhibitory responses, but instead a possible shift in inhibitory processing in the dorsal striatal circuitry.

PNNs consist of chondroitin sulfate proteoglycans (55–59) and are known to regulate plasticity (30,31,60). Our observed increase in percentage of PV+ cells with PNNs in mouse models of excessive repetitive behaviors is consistent with the proposed role that PNNs modulate inhibitory plasticity. PNNs in the mouse visual cortex are associated with increased firing of PV+ inhibitory interneurons (61) and have been linked to neuronal oscillations in other brain regions (62–64), suggesting that they play a role in modulating coordinated network activity. Our results suggest that abnormal PV+ PNNs in the DMS contribute to altered neuronal oscillations, specifically within the theta frequency. PV+ interneurons in the striatum are known to fire in synchrony (65–67), and evidence suggests that neuronal synchrony in the striatum is important for healthy function. In the healthy rodent striatum, theta power is associated with voluntary behavior and does not appear to be associated with grooming (49). In pathological states, however, altered theta and gamma power have been linked to overgrooming (68,69), raising the possibility that the increased oscillations in the theta range we observed in BTBR mice may be causally linked to excessive grooming. Along these lines, high theta power has been observed in humans with obsessive-compulsive disorder and trichotillomania (70–74), both conditions defined by dysfunctional repetitive behavior. Future studies should investigate whether reducing the percentage of PV+ cells with PNNs would normalize DMS oscillations in BTBR mice.

Inhibitory input from small numbers of PV+ interneurons is sufficient to block firing in large numbers of MSNs (20). Therefore, we examined whether PV+ PNNs may impact inhibitory responses of DMS MSNs. We found that DMS MSNs are atypical in BTBR mice, exhibiting fewer dendritic spines in combination with electrophysiological changes that suggest higher inhibitory postsynaptic responses compared with control mice. Given this information, we hypothesized that concomitant decreases in excitatory synapses and increases in inhibitory transmission on DMS MSNs in BTBR mice contribute to excessive grooming and digging.

To extend our understanding of how PNNs might affect DMS MSNs in BTBR mice, mIPSCs were recorded from striatal slices at baseline and after reducing DMS PNNs with chABC. Given that reducing PNNs in BTBR mice eliminated excessive repetitive behaviors, we expected to find baseline differences between BTBR and control mice in mIPSC measures that would be sensitive to PNN reduction. Baseline data suggested an increase in BTBR spontaneous GABA release onto putative MSN cell bodies, as well as potentially more inhibitory postsynaptic receptors on MSNs. This difference was not corrected after chABC treatment, and instead degrading PNNs resulted in an unexpected increase in inhibitory presynaptic strength in BTBR MSNs compared with control MSNs. Similarly, a previous study investigating spontaneous excitatory and inhibitory transmission onto CA2 fast-spiking interneurons of control mice, 7 dpi of chABC, found that reducing PNNs decreased the frequency of excitatory events and increased the frequency of inhibitory events onto fast-spiking interneurons (75). In addition, although in our electrophysiology experiments we did not measure excitatory postsynaptic responses, our dendritic spine results may provide insight into excitatory synaptic plasticity effects after reducing PNNs. The changes we observed likely resemble a complex reorganization of inhibitory circuit strength, perhaps influenced by other endogenous physiological differences between mouse strains. While we cannot be certain if this directly reflects modulation of MSNs by PV+ interneurons, it is possible that concomitant inhibitory signaling is altered in BTBR mice as a result of PNN decreases around PV+ interneurons. PNN reduction increased mIPSC frequency in BTBR mice, in addition to maintaining increased mIPSC amplitude. While these findings are surprising given past work showing that PNN degradation reduces inhibition in several brain regions (76,77), it is important to note that in the cerebellum where, similar to the striatum, circuits are predominantly inhibitory, PNN degradation also increases inhibition (78,79).

It is noteworthy that some of the measures we considered were affected by treatment with the control enzyme, pnase. In particular, treatment with either pnase or chABC restored dendritic spine density on MSNs, and some of the behavioral differences between C57 and BTBR mice were diminished with pnase treatment. While the exact reason for these unexpected findings remains unknown, it may be relevant that a growing number of studies have shown that commonly used anesthetics, including isoflurane, can enhance plasticity and reverse negative stress-induced behavioral outcomes (80,81). Future studies should investigate this possibility directly.

Recent work suggesting that PV+ cell activity drives the formation of PNNs (82,83) raises the possibility that higher percentages of PV+ interneurons with PNNs in the mouse models we examined are caused by excessive repetitive behavior. While our chABC data indicate that the converse relationship exists, both possibilities may occur. That is, a positive feedback loop may exist whereby high numbers of PV+ interneurons with PNNs stimulate increased grooming and digging, which in turn reinforce PNNs surrounding PV+ interneurons, ensuring the persistence of maladaptive behavior. Collectively, our findings suggest that an overabundance of PNNs surrounding PV+ interneurons in the DMS may prevent disengagement from repetitive behaviors through abnormal inhibitory signaling between PV+ interneurons and MSNs.

ACKNOWLEDGMENTS AND DISCLOSURES

This work was supported by the National Institutes of Health (Grant No. 1R01 MH118631-01 [to EG]), Simons Foundation Autism Research Initiative Pilot Award (Grant No. 670183 [to TJB]), New York Stem Cell Foundation (to IBW), National Science Foundation Graduate Research Fellowship Program (to BAB and WTF), and National Institutes of Health National Center for Advancing Translational Sciences Award (Grant No. TL1TR003019 [to CJM]).

We thank the Gould Laboratory members for helpful discussions on the project.

The authors report no biomedical financial interests or potential conflicts of interest.

ARTICLE INFORMATION

From the Princeton Neuroscience Institute, Princeton University, Princeton, New Jersey.

MNP and WTF contributed equally to this work.

Address correspondence to Elizabeth Gould, Ph.D., at goulde@princeton.edu.

Received Aug 23, 2021; revised Oct 29, 2021; accepted Nov 3, 2021.

Supplementary material cited in this article is available online at https://doi.org/10.1016/j.bpsgos.2021.11.005.

REFERENCES

1. National Institute of Mental Health: Autism spectrum disorder (ASD) Available at: https://www.nimh.nih.gov/health/statistics/autism-spectrum-disorder-asd.shtml. Accessed August 27, 2020.
2. Hollander E, Greenwald S, Neville D, Johnson J, Hornig CD, Weissman MM (1996): Uncomplicated and comorbid obsessive-compulsive disorder in an epidemiologic sample. Depress Anxiety 4:111–119.
3. Penadés R, Catalán R, Andrés S, Salamero M, Gastó C (2005): Executive function and nonverbal memory in obsessive-compulsive disorder. Psychiatry Res 133:81–90.
4. Centers for Disease Control and Prevention: Data and Statistics on Autism Spectrum Disorder Available at: https://www.cdc.gov/ncbddd/autism/data.html. Accessed August 27, 2020.
5. Shin NY, Lee TY, Kim E, Kwon JS (2014): Cognitive functioning in obsessive-compulsive disorder: A meta-analysis. Psychol Med 44:1121–1130.
6. Knowlton BJ, Mangels JA, Squire LR (1996): A neostriatal habit learning system in humans. Science 273:1399–1402.
7. Langen M, Schnack HG, Nederveen H, Bos D, Lahuis BE, de Jonge MV, *et al.* (2009): Changes in the developmental trajectories of striatum in autism. Biol Psychiatry 66:327–333.
8. Langen M, Durston S, Kas MJH, van Engeland H, Staal WG (2011): The neurobiology of repetitive behavior:… and men. Neurosci Biobehav Rev 35:356–365.
9. Abbott AE, Linke AC, Nair A, Jahedi A, Alba LA, Keown CL, *et al.* (2018): Repetitive behaviors in autism are linked to imbalance of corticostriatal connectivity: A functional connectivity MRI study. Soc Cogn Affect Neurosci 13:32–42.
10. Ahmari SE, Spellman T, Douglass NL, Kheirbek MA, Simpson HB, Deisseroth K, *et al.* (2013): Repeated cortico-striatal stimulation generates persistent OCD-like behavior. Science 340:1234–1239.
11. Burguière E, Monteiro P, Feng G, Graybiel AM (2013): Optogenetic stimulation of lateral orbitofronto-striatal pathway suppresses compulsive behaviors. Science 340:1243–1246.
12. Burguière E, Monteiro P, Mallet L, Feng G, Graybiel AM (2015): Striatal circuits, habits, and implications for obsessive-compulsive disorder. Curr Opin Neurobiol 30:59–65.
13. Chang HT, Wilson CJ, Kitai ST (1982): A Golgi study of rat neostriatal neurons: Light microscopic analysis. J Comp Neurol 208:107–126.
14. Bolam JP, Hanley JJ, Booth PA, Bevan MD (2000): Synaptic organisation of the basal ganglia. J Anat 196(Pt 4):527–542.
15. Hjorth JJJ, Kozlov A, Carannante I, Nylén JF, Lindroos R, Johansson Y, *et al.* (2020): The microcircuits of striatum in silico. Proc Natl Acad Sci U S A 117:9554–9565.
16. Cowan RL, Wilson CJ, Emson PC, Heizmann CW (1990): Parvalbumin-containing GABAergic interneurons in the rat neostriatum. J Comp Neurol 302:197–205.
17. Kita H (1993): GABAergic circuits of the striatum. Prog Brain Res 99:51–72.
18. Kita H, Kosaka T, Heizmann CW (1990): Parvalbumin-immunoreactive neurons in the rat neostriatum: A light and electron microscopic study. Brain Res 536:1–15.
19. Gittis AH, Nelson AB, Thwin MT, Palop JJ, Kreitzer AC (2010): Distinct roles of GABAergic interneurons in the regulation of striatal output pathways. J Neurosci 30:2223–2234.
20. Lee K, Holley SM, Shobe JL, Chong NC, Cepeda C, Levine MS, *et al.* (2017): Parvalbumin interneurons modulate striatal output and enhance performance during associative learning. Neuron 93:1451–1463.e4.
21. Lee H, Leamey CA, Sawatari A (2012): Perineuronal nets play a role in regulating striatal function in the mouse. PLoS One 7:e32747.
22. Derouiche A, Härtig W, Brauer K, Brückner G (1996): Spatial relationship of lectin-labelled extracellular matrix and glutamine synthetase-immunoreactive astrocytes in rat cortical forebrain regions. J Anat 189:363–372.
23. Pizzorusso T, Medini P, Berardi N, Chierzi S, Fawcett JW, Maffei L (2002): Reactivation of ocular dominance plasticity in the adult visual cortex. Science 298:1248–1251.
24. Gogolla N, Caroni P, Lüthi A, Herry C (2009): Perineuronal nets protect fear memories from erasure. Science 325:1258–1261.
25. Frischknecht R, Heine M, Perrais D, Seidenbecher CI, Choquet D, Gundelfinger ED (2009): Brain extracellular matrix affects AMPA receptor lateral mobility and short-term synaptic plasticity. Nat Neurosci 12:897–904.
26. Miyata S, Komatsu Y, Yoshimura Y, Taya C, Kitagawa H (2012): Persistent cortical plasticity by upregulation of chondroitin 6-sulfation. Nat Neurosci 15:414–422.
27. Favuzzi E, Marques-Smith A, Deogracias R, Winterflood CM, Sánchez-Aguilera A, Mantoan L, *et al.* (2017): Activity-dependent gating of parvalbumin interneuron function by the perineuronal net protein brevican. Neuron 95:639–655.e10.
28. Rankin-Gee EK, McRae PA, Baranov E, Rogers S, Wandrey L, Porter BE (2015): Perineuronal net degradation in epilepsy. Epilepsia 56:1124–1133.
29. Yang S, Cacquevel M, Saksida LM, Bussey TJ, Schneider BL, Aebischer P, *et al.* (2015): Perineuronal net digestion with chondroitinase restores memory in mice with tau pathology. Exp Neurol 265:48–58.
30. Sorg BA, Berretta S, Blacktop JM, Fawcett JW, Kitagawa H, Kwok JCF, *et al.* (2016): Casting a wide net: Role of perineuronal nets in neural plasticity. J Neurosci 36:11459–11468.
31. Pantazopoulos H, Berretta S (2016): In sickness and in health: Perineuronal nets and synaptic plasticity in psychiatric disorders. Neural Plast 2016:9847696.
32. Skaar DA, Shao Y, Haines JL, Stenger JE, Jaworski J, Martin ER, *et al.* (2005): Analysis of the RELN gene as a genetic risk factor for autism. Mol Psychiatry 10:563–571.
33. Carayol J, Sacco R, Tores F, Rousseau F, Lewin P, Hager J, *et al.* (2011): Converging evidence for an association of ATP2B2 allelic variants with autism in male subjects. Biol Psychiatry 70:880–887.
34. Guzman SJ, Schlögl A, Schmidt-Hieber C (2014): Stimfit: quantifying electrophysiological data with Python. Front Neuroinform 8(16). https://doi.org/10.3389/fninf.2014.00016.
35. Briones BA, Tang VD, Haye AE, Gould E (2018): Response learning stimulates dendritic spine growth on dorsal striatal medium spiny neurons. Neurobiol Learn Mem 155:50–59.
36. Schindelin J, Arganda-Carreras I, Frise E, Kaynig V, Longair M, Pietzsch T, *et al.* (2012): Fiji: an open-source platform for biological-image analysis. Nature Methods 9:676–682.
37. Peça J, Feliciano C, Ting JT, Wang W, Wells MF, Venkatraman TN, *et al.* (2011): Shank3 mutant mice display autistic-like behaviours and striatal dysfunction. Nature 472:437–442.
38. Peñagarikano O, Abrahams BS, Herman EI, Winden KD, Gdalyahu A, Dong H, *et al.* (2011): Absence of CNTNAP2 leads to epilepsy, neuronal migration abnormalities, and core autism-related deficits. Cell 147:235–246.
39. Roullet FI, Lai JK, Foster JA (2013): In utero exposure to valproic acid and autism—a current review of clinical and animal studies. Neurotoxicol Teratol 36:47–56.
40. Meyza KZ, Blanchard DC (2017): The BTBR mouse model of idiopathic autism—current view on mechanisms. Neurosci Biobehav Rev 76:99–110.
41. Cai Y, Wang L, Xiao R, Li X, He X, Gao J, *et al.* (2017): Autism-like behavior in the BTBR mouse model of autism is improved by propofol. Neuropharmacology 118:175–187.
42. Nicolini C, Fahnestock M (2018): The valproic acid-induced rodent model of autism. Exp Neurol 299:217–227.
43. Amodeo DA, Jones JH, Sweeney JA, Ragozzino ME (2014): Risperidone and the 5-HT2A receptor antagonist M100907 improve

probabilistic reversal learning in BTBR T + tf/J mice. Autism Res 7:555–567.
44. Kim KC, Gonzales EL, Lázaro MT, Choi CS, Bahn GH, Yoo HJ, *et al.* (2016): Clinical and neurobiological relevance of current animal models of autism spectrum disorders. Biomol Ther 24:207–243.
45. Wei D, Dinh D, Lee D, Li D, Anguren A, Moreno-Sanz G, *et al.* (2016): Enhancement of anandamide-mediated endocannabinoid signaling corrects autism-related social impairment. Cannabis Cannabinoid Res 1:81–89.
46. Cabungcal JH, Steullet P, Morishita H, Kraftsik R, Cuenod M, Hensch TK, *et al.* (2013): Perineuronal nets protect fast-spiking interneurons against oxidative stress. Proc Natl Acad Sci U S A 110:9130–9135.
47. Yamada J, Ohgomori T, Jinno S (2015): Perineuronal nets affect parvalbumin expression in GABAergic neurons of the mouse hippocampus. Eur J Neurosci 41:368–378.
48. Slaker M, Churchill L, Todd RP, Blacktop JM, Zuloaga DG, Raber J, *et al.* (2015): Removal of perineuronal nets in the medial prefrontal cortex impairs the acquisition and reconsolidation of a cocaine-induced conditioned place preference memory. J Neurosci 35:4190–4202.
49. DeCoteau WE, Thorn C, Gibson DJ, Courtemanche R, Mitra P, Kubota Y, *et al.* (2007): Oscillations of local field potentials in the rat dorsal striatum during spontaneous and instructed behaviors. J Neurophysiol 97:3800–3805.
50. Thorn CA, Graybiel AM (2014): Differential entrainment and learning-related dynamics of spike and local field potential activity in the sensorimotor and associative striatum. J Neurosci 34:2845–2859.
51. Bennett BD, Bolam JP (1994): Synaptic input and output of parvalbumin-immunoreactive neurons in the neostriatum of the rat. Neuroscience 62:707–719.
52. Hunnicutt BJ, Jongbloets BC, Birdsong WT, Gertz KJ, Zhong H, Mao T (2016): A comprehensive excitatory input map of the striatum reveals novel functional organization. eLife 5:e19103.
53. Selemon LD, Goldman-Rakic PS (1985): Longitudinal topography and interdigitation of corticostriatal projections in the rhesus monkey. J Neurosci 5:776–794.
54. Kötter R (1994): Postsynaptic integration of glutamatergic and dopaminergic signals in the striatum. Prog Neurobiol 44:163–196.
55. Nikonenko I, Jourdain P, Muller D (2003): Presynaptic remodeling contributes to activity-dependent synaptogenesis. J Neurosci 23:8498–8505.
56. Dityatev A, Brückner G, Dityateva G, Grosche J, Kleene R, Schachner M (2007): Activity-dependent formation and functions of chondroitin sulfate-rich extracellular matrix of perineuronal nets. Dev Neurobiol 67:570–588.
57. Gurevicius K, Kuang F, Stoenica L, Irintchev A, Gureviciene I, Dityatev A, *et al.* (2009): Genetic ablation of tenascin-C expression leads to abnormal hippocampal CA1 structure and electrical activity in vivo. Hippocampus 19:1232–1246.
58. Miyata S, Kitagawa H (2016): Chondroitin 6-sulfation regulates perineuronal net formation by controlling the stability of aggrecan. Neural Plast 2016:1305801.
59. Gottschling C, Wegrzyn D, Denecke B, Faissner A (2019): Elimination of the four extracellular matrix molecules tenascin-C, tenascin-R, brevican and neurocan alters the ratio of excitatory and inhibitory synapses. Sci Rep 9:13939.
60. Bosiacki M, Gąssowska-Dobrowolska M, Kojder K, Fabiańska M, Jeżewski D, Gutowska I, *et al.* (2019): Perineuronal nets and their role in synaptic homeostasis. Int J Mol Sci 20:4108.
61. Faini G, Aguirre A, Landi S, Lamers D, Pizzorusso T, Ratto GM, *et al.* (2018): Perineuronal nets control visual input via thalamic recruitment of cortical PV interneurons. eLife 7:e41520.
62. Steullet P, Cabungcal JH, Cuénod M, Do KQ (2014): Fast oscillatory activity in the anterior cingulate cortex: dopaminergic modulation and effect of perineuronal net loss. Front Cell Neurosci 8:244.
63. Lensjø KK, Lepperød ME, Dick G, Hafting T, Fyhn M (2017): Removal of perineuronal nets unlocks juvenile plasticity through network mechanisms of decreased inhibition and increased gamma activity. J Neurosci 37:1269–1283.
64. Wingert JC, Sorg BA (2021): Impact of perineuronal nets on electrophysiology of parvalbumin interneurons, principal neurons, and brain oscillations: A review. Front Synaptic Neurosci 13:673210.
65. Gittis AH, Hang GB, LaDow ES, Shoenfeld LR, Atallah BV, Finkbeiner S, *et al.* (2011): Rapid target-specific remodeling of fast-spiking inhibitory circuits after loss of dopamine. Neuron 71:858–868.
66. Sharott A, Doig NM, Mallet N, Magill PJ (2012): Relationships between the firing of identified striatal interneurons and spontaneous and driven cortical activities in vivo. J Neurosci 32:13221–13236.
67. von Nicolai C, Engler G, Sharott A, Engel AK, Moll CK, Siegel M (2014): Corticostriatal coordination through coherent phase-amplitude coupling. J Neurosci 34:5938–5948.
68. Dzirasa K, Phillips HW, Sotnikova TD, Salahpour A, Kumar S, Gainetdinov RR, *et al.* (2010): Noradrenergic control of cortico-striato-thalamic and mesolimbic cross-structural synchrony. J Neurosci 30:6387–6397.
69. Dhamne SC, Silverman JL, Super CE, Lammers SHT, Hameed MQ, Modi ME, *et al.* (2017): Replicable in vivo physiological and behavioral phenotypes of the *Shank3B* null mutant mouse model of autism. Mol Autism 8:26.
70. Kamaradova D, Hajda M, Prasko J, Taborsky J, Grambal A, Latalova K, *et al.* (2016): Cognitive deficits in patients with obsessive-compulsive disorder—electroencephalography correlates. Neuropsychiatr Dis Treat 12:1119–1125.
71. Rappel P, Marmor O, Bick AS, Arkadir D, Linetsky E, Castrioto A, *et al.* (2018): Subthalamic theta activity: A novel human subcortical biomarker for obsessive compulsive disorder. Transl Psychiatry 8:118.
72. Miller KJ, Prieto T, Williams NR, Halpern CH (2019): Case studies in neuroscience: The electrophysiology of a human obsession in nucleus accumbens. J Neurophysiol 121:2336–2340.
73. Buot A, Karachi C, Lau B, Belaid H, Fernandez-Vidal S, Welter ML, *et al.* (2021): Emotions modulate subthalamic nucleus activity: New evidence in obsessive-compulsive disorder and Parkinson's disease patients. Biol Psychiatry Cogn Neurosci Neuroimaging 6:556–567.
74. Peris TS, Salgari G, Perez J, Jurgiel J, Vreeland A, O'Neill J, *et al.* (2021): Shared and unique neural mechanisms underlying pediatric trichotillomania and obsessive compulsive disorder. Psychiatry Res 298:113653.
75. Hayani H, Song I, Dityatev A (2018): Increased excitability and reduced excitatory synaptic input into fast-spiking CA2 interneurons after enzymatic attenuation of extracellular matrix. Front Cell Neurosci 12:149.
76. Balmer TS (2016): Perineuronal nets enhance the excitability of fast-spiking neurons. eNeuro 3. ENEURO.0112-16.2016.
77. Alaiyed S, McCann M, Mahajan G, Rajkowska G, Stockmeier CA, Kellar KJ, *et al.* (2020): Venlafaxine stimulates an MMP-9-dependent increase in excitatory/inhibitory balance in a stress model of depression. J Neurosci 40:4418–4431.
78. Hirono M, Watanabe S, Karube F, Fujiyama F, Kawahara S, Nagao S, *et al.* (2018): Perineuronal nets in the deep cerebellar nuclei regulate GABAergic transmission and delay eyeblink conditioning. J Neurosci 38:6130–6144.
79. Carulli D, Broersen R, de Winter F, Muir EM, Mešković M, de Waal M, *et al.* (2020): Cerebellar plasticity and associative memories are controlled by perineuronal nets. Proc Natl Acad Sci U S A 117:6855–6865.
80. Antila H, Ryazantseva M, Popova D, Sipilä P, Guirado R, Kohtala S, *et al.* (2017): Isoflurane produces antidepressant effects and induces TrkB signaling in rodents. Sci Rep 7:7811.
81. Zhang SS, Tian YH, Jin SJ, Wang WC, Zhao JX, Si XM, *et al.* (2019): Isoflurane produces antidepressant effects inducing BDNF-TrkB signaling in CUMS mice. Psychopharmacology 236:3301–3315.
82. Cisneros-Franco JM, de Villers-Sidani É. (2019): Reactivation of critical period plasticity in adult auditory cortex through chemogenetic silencing of parvalbumin-positive interneurons. Proc Natl Acad Sci U S A 116:26329–26331.
83. Devienne G, Picaud S, Cohen I, Piquet J, Tricoire L, Testa D, *et al.* (2021): Regulation of perineuronal nets in the adult cortex by the activity of the cortical network. J Neurosci 41:5779–5790.